International Journal of Biological Macromolecules 372 (2026) 152929

Contents lists available at ScienceDirect

International Journal of Biological Macromolecules

journal homepage: www.elsevier.com/locate/ijbiomac

The motility of *B. subtilis* determines the timescale of the antimicrobial action of chitosan-based hydrogels

F. Soto-Bustamante, G. Bassu, M. Laurati *

Department of Chemistry, University of Florence, via della Lastruccia 3, Sesto Fiorentino, 50019, Italy
Consorzio interuniversitario per lo sviluppo dei Sistemi a Grande Interfase (CSGI), via della Lastruccia 3, Sesto Fiorentino, 50019, Italy

ARTICLE INFO

Keywords:
Bacterial motility
Antimicrobial hydrogels
Chitosan
Particle tracking
Anomalous diffusion

ABSTRACT

We study the motility of *B. subtilis* confined within antimicrobial Chitosan(CT)-Polyvinylalcohol(PVA) porous hydrogels using confocal microscopy and particle tracking. We show that with increasing CT content the bacterial motility reduces, as indicated by the average mean squared displacements (MSDs), and the mean bacterial velocities. Furthermore, the short-time motility changes qualitatively from the straight runs characteristic of the run-and-tumble motility to diffusion and sub-diffusion. In the anomalous diffusion regime a large spread of individual MSDs indicates the presence of pronounced dynamical heterogeneities. At the same time the ergodicity breaking parameter presents a maximum at small CT content. We interpret these findings in terms of a competition between confinement effects and the electrostatic interactions between bacteria and hydrogel, with the former being important at small CT contents, and leading to a broadening of the motility distribution, while the latter dominating at larger CT fractions and inducing slower but more homogeneous dynamics. We show that the effects on motility are the first stage of the antimicrobial action, that occurs on a timescale that depends on CT content and determines the onset of bacterial damage. Our results thus show that CT content tunes both the strength and the timescale of antimicrobial action.

1. Introduction

Chitosan (CT) is an abundant natural polysaccharide obtained from chitin by deacetylation or enzymatic treatment of chitin deacetylase. It is non-toxic and biodegradable and presents antioxidant [1], anti-inflammatory [2], hemostatic activities [3], and antimicrobial action [4]. It is therefore widely exploited in applications such as drug delivery [5], wound healing [6], tissue engineering [7] and food preservation [8].

Different antimicrobial mechanisms of action of Chitosan have been reported [9–12]: The most recognized one is associated with the electrostatic interaction between the NH_3 functional groups of Chitosan and anionic structures on the bacterial membrane, such as lipopolysaccharides and proteins. This electrostatically induced binding changes membrane permeability, disrupting normal cellular function, finally leading to lysis. An additional antimicrobial mechanism is related to the deposition of Chitosan on the bacterial membrane: such deposition creates a polymeric envelope on the surface of the bacteria, affecting the uptake of nutrients and the disposal of waste materials, thus inducing the death of the bacteria. Another mechanism is associated with the ability of Chitosan to chelate divalent cations: since these ions are stabilizing the bacterial membrane, their capture by Chitosan also results in membrane disruption [13–15]. Finally, it has been also suggested that Chitosan nanoparticles can affect the motility of flagella [16,17], and therefore induce immobilization and death.

Among different CT-based materials, hydrogels [18] have been also exploited for their antimicrobial properties in food packaging [19] and as films for wound healing [20], among others [18]. When bacteria are penetrating a CT-based hydrogel, the electrostatic attraction between the positively charged CT surface and the negatively charged bacterial membrane is responsible for bacterial trapping on the surface of the hydrogel [21], where subsequently the antimicrobial action occurs. However, details of the early stage electrostatic interaction between bacteria and CT-based hydrogels, how this is modulated by CT content and what is the timescale of the electrostatic trapping, are essentially unexplored. Furthermore, the interplay between confinement effects and electrostatic interaction is unclear. All these aspect are important to fully understand, control and design the antimicrobial activity of CT-based hydrogels.

We address here these questions by investigating the interaction of a gram positive bacterium exhibiting run-and-tumble motility [22,23], *B. subtilis*, absorbed within polyvinylalcohol/chitosan hydrogels containing different amounts of CT. We show that while the pores in the

* Corresponding author at: Department of Chemistry, University of Florence, via della Lastruccia 3, Sesto Fiorentino, 50019, Italy.
E-mail address: marco.laurati@unifi.it (M. Laurati).

https://doi.org/10.1016/j.ijbiomac.2026.152929
Received 11 February 2026; Received in revised form 3 June 2026; Accepted 5 June 2026
Available online 13 June 2026

hydrogels are becoming larger with increasing CT content, i.e. potential confinement effects are reduced, the increasing electrostatic attraction leads to anomalous diffusion prior to trapping and bacterial damage. Anomalous diffusion, i.e. a motion in which the mean squared displacement shows a power-law dependence on time with exponent $n \neq 1$, has been observed in many different systems, including the cellular environment, polymer nanocomposites, confined passive and active particles [24,25]. By determining various parameters of the observed anomalous diffusion we investigate its origin, and we show that the amount of CT finely tunes the deviation from active run-and-tumble motion and the timescale of the electrostatic entrapment on the hydrogel surface, thus affecting in turn the timescale of the antimicrobial action. These findings show therefore that bacterial motility can be used as a parameter to investigate the time-dependent antimicrobial action of the hydrogels.

2. Materials and methods

We describe in what follows the procedure to prepare the gels, their characterization, the preparation of the bacterial colonies and their incorporation in the gels, the microscopy experiments and their analysis. A scheme describing all these steps from sample preparation to microscopy experiments is reported in Fig.1 of the Supplementary material (SM).

2.1. Gel preparation

CT with molecular weight $M_w = 190 - 300$ KDa, PVA with $M_w = 146 - 186$ KDa and with a degree of hydrolization equal to 99 + %, and acetic acid were purchased from Merck, and used without further purification. CT was dissolved at temperature T = 20° C in a solution of acetic acid and milli-Q water (0.1 M) at a concentration of 2% (w/v). The solution was continuously mixed for 4 h using a magnetic stirrer. PVA was dissolved in milli-Q water at a concentration of 5% (w/v) and at $T = 90$ °C, mixing for 1 h with a magnetic stirrer. The so-obtained CT and PVA solutions were mixed for 1 h at $T = 50$ °C in different volume ratios: PVA100%-CT0%, PVA90%-CT10%, PVA80%-CT20%, PVA70%-CT30%, PVA60%-CT40%, PVA50%-CT50% and PVA30%-CT70%. After mixing the solutions were poured into a Petri dish. Freeze-thawing was used to induce physical crosslinking and formation of hydrogels. Freezing was performed at $T = -20$ °C, while thawing at room temperature, for a total of 3 cycles, each one consisting of 24 h (freezing and thawing). Since in previous work [26] no pronounced differences were found between distinct freeze-thawing ratios, we used a 12 h freezing and a 12 h thawing times. The obtained hydrogels were washed every 12 h with milli-Q water for a total of 4 days to remove any non-crosslinked polymer residue in the sample. Fluorescent labeling was obtained by immersing the hydrogels in a solution of Rhodamine B for 72 h. The long immersion time was used to obtain a uniform distribution of fluorescent dye within the hydrogel. Due to the strong affinity between Rhodamine B and the used polymers, the amount of dye in the liquid phase of the swollen hydrogels is negligible.

2.2. Characterization of gel porosity

To characterize the gel porosity, confocal microscopy imaging was carried out on fluorescently labeled, fully hydrated hydrogel samples by using a Leica TCS SP8 confocal microscope. Samples were deposited on the wells of LabTek Chambered Coverglass with a 1.0 borosilicate glass coverslip at the bottom, and imaged using a 63× oil immersion objective with a numerical aperture N.A. = 1.43. A 561 nm wavelength laser was used to excite Rhodamine B and the fluorescence emission was collected through a hybrid GaAsp detector over a wavelength spectrum from 571 to 600 nm. For each sample we collected 10 volume stacks of 512 × 512 × 251 pixels^3, corresponding to hydrogel volumes of 184 × 184 × 50 μm^3, at 15 μm distance from the coverslip. Three replicates were measured for each gel.

MorphoLibJ [27] was used to process and analyze the obtained volume stacks. In particular, the software was used to determine the pores present in the imaged volume of the hydrogels, and to estimate an average pore radius R as follows: Inertia ellipsoids were fit within each pore, and their axes R_x, R_y, and R_z were extracted. Then $R_j = (R_x+R_y+R_z/3)$ was calculated for each pore j, and its average value R and standard deviation were determined using the data obtained from 10 volumes and 3 replicates. Pores on the edges of the imaged volumes were excluded from the analysis since these may extend beyond it. In principle the individual pore volumes and total volume fraction could be also estimated from the image analysis. However, due to the limited resolution and statistics, we preferred to use swelling data to determine gel porosity according to:

$$\phi(\%) = \frac{\frac{W_s - W_d}{\rho_{water}}}{\frac{W_s - W_d}{\rho_{water}} + \frac{W_d}{\rho_{polymer}}} \times 100 \quad (1)$$

The average ϕ was obtained as the mean of three replicates, and errors as the maximum deviation from the mean.

2.3. Bacterial culture

Bacillus subtilis (type strain DMS-10) was purchased from DMSZ (Germany). The bacterial culture was re-activated according to the procedure provided by DMSZ [28,29], and subsequently diluted in tryptic soy broth (TSB) to obtain a dispersion presenting an optical density of approximately 1, as measured using a Thermo Scientific NanoDrop OneC UV–Vis Spectrophotometer with a wavelength of 600 nm (OD_{600}). Colonies for the individual experiments were prepared by inoculating aliquotes in 5 mL TSB at 32 °C, that were then growing overnight while agitated at 180 rpm. Measurements of OD_{600} at intervals of 30 min were used to confirm that the stationary phase was achieved. Once in the stationary phase, the bacterial dispersion was diluted to OD_{600}= 0.15 in fresh TSB and additional growth was induced over 30 min. This procedure allowed maximization of the number of motile cells. Bacteria were fluorescently labeled by adding a solution of SYTO9 to the bacterial dispersion with a final concentration of 5 μM. The dispersion was then kept in the dark for 15 min under mild agitation. In the bacterial dispersion used for the confocal microscopy experiments the concentration was sufficiently low to neglect local gradients of oxygen or nutrient, and to avoid significant differences in bacteria interactions throughout the sample.

2.4. Adsorption of bacteria within the hydrogels

Hydrogels were preliminary equilibrated in fresh TSB overnight in sterile vials to avoid any possible gradient in nutrient or oxygen concentration. To induce bacteria adsorption, 200 μL of bacterial dispersion were poured in the wells of a Labtek sterile plate; in a second step, the previously equilibrated hydrogels were inserted in the wells containing the bacterial dispersion for 15 min, under soft agitation and in the dark.

2.5. Tracking of bacterial motions and analysis of trajectories

The motility of the bacteria in bulk and absorbed within the hydrogels was determined through particle tracking analysis applied to time series of confocal microscopy images acquired with the Leica TSC SP8 microscope. The fluorescence from the polymer network of the hydrogel (Rhodamine B) was again excited using a 561 nm wavelength laser, while the fluorescence of the bacteria (SYTO9) was excited using a 488 nm laser. The corresponding fluorescence emissions were detected using two GaAsp hybrid detectors in the wavelength ranges 571–600 nm (hydrogel) and 498–550 nm (bacteria). For each

sample 2000 images of 512 × 512 pixels^2, corresponding to a sample area of 42 × 42 μm^2, were acquired at room temperature with a rate of 27.8 fps. Particle tracking analysis of the obtained image time series was performed using Trackpy v0.50 [30,31]. Particle trajectories were corrected for background drift using routines available in Trackpy. The ensemble-averaged, time-averaged mean squared displacement was calculated in Trackpy according to the following expression:

$$\langle \Delta r^2(\tau)\rangle = \langle \overline{\delta r_i^2(\tau)}\rangle_i \tag{2}$$

where τ is the lag-time, $\langle\,\rangle_i$ indicates an average over all trajectories i and $\overline{\Delta r_i^2(\tau)}$ is the time-averaged MSD of trajectory i:

$$\overline{\delta r_i^2(\tau)} = \overline{|x_i(t+\tau) - x_i(t)|^2 + |y_i(t+\tau) - y_i(t)|^2} \tag{3}$$

where x_i and y_i are the coordinates of the centroid of bacterium i, t is the time along the trajectory, and the overline indicates the time-average. Errors on $\langle \Delta r^2(\tau)\rangle$ were calculated as standard deviations. The deviation of individual time-averaged MSDs from their ensemble-average for a lag-time τ was calculated as:

$$\xi(\tau) = \overline{\delta r_i^2(\tau)}/\langle \Delta r^2(\tau)\rangle \tag{4}$$

and the variance of the distribution of $\xi(\tau)$ values, also called ergodicity breaking parameter EB, was calculated according to:

$$EB = \langle \xi^2(\tau)\rangle - \langle \xi(\tau)\rangle^2 \tag{5}$$

TrackMate was additionally used to analyze single trajectories and extract their characteristic speeds and distributions [32–34].

3. Results and discussion

3.1. Characterization of the gel network structure and mechanical properties

The gel network structure as a function of composition and the mechanical properties of the gels were characterized in detail in previous work [26]. We briefly report here the main findings of this characterization, referring to the cited reference for additional details. The network structure was investigated by scanning electron microscopy (SEM) and small angle X-ray scattering (SAXS). SAXS data were modeled assuming a fractal network structure of the gel, obtaining as a result that the average mesh size is of order 3–4 nm and is poorly dependent on the composition (CT content). At the same time, solid-like heterogeneities of the network become smaller with increasing CT content, i.e. the gel becomes more homogeneous as confirmed by SEM images. This is also indicated by the increase in hydrogel transparency with increasing CT content (Fig. 1, left). Rheological measurements of the gels showed a progressive softening of the network with increasing CT content, as a result of the lower compliance of the CT network with respect to the pure PVA network.

3.2. Characterization of gel porosity

In this section we discuss the characterization of the gel porosity obtained from the analysis of confocal microscopy image stacks. Fig. 1(top) reports exemplary renderings of gel networks with CT contents equal to 0%, 30% and 70%, renderings for the remaining compositions can be found in Fig.2 of the SM. The heterogeneous porous structure of the gels is evident in all cases. The pore morphology and size was analyzed using Morpholibj, as described in Materials and Methods and as previously described in detail [26]. By modeling pores using inscribed ellipsoids, their morphology was found to be asymmetric. Referring to the axes in Fig. 1 (top), it was found that the pores are elongated in the y-direction for a section along the x-y plane, while relatively flat in the vertical direction z [26]. As shown in Fig. 1(bottom) the average pore size, determined as described in Section 2.2, increases with increasing CT content, in particular above 40% [35,36]. On the other hand, the corresponding distributions of pore volumes are broad for CT contents < 40%, while they become narrower for larger CT contents [26]. The increase in pore size is reflected in an increase of the porosity ϕ as a function of chitosan content (Fig. 1, inset).

3.3. Bacterial motility

We analyze in this section the results regarding the motility of bacteria absorbed within PVA-CT hydrogels with varying CT content. We first discuss the ensemble average of the time averaged mean squared displacements (ETAMSD) and their variation with CT content, and later report a detailed analysis of the individual time-averaged MSDs (TAMSD) (Eq. (3)) and their distribution, discussing our results in the framework of available models for anomalous diffusion. The ETAMSDs were obtained according to Eq. (2) averaging about 300 trajectories up to 30% CT content, about 250 for 40% CT content, and 150 for larger CT contents.

3.3.1. Ensemble averaged, time averaged MSD

The motility of freely swimming *B. subtilis* can be described in terms of the run and tumble model [23,37,38]. The characteristic directed motion associated with the run phase can be clearly seen in the exemplary trajectories reported in Fig. 2A (left) for *B.subtilis* in triptic soy broth buffer. The corresponding ETAMSD is characterized at short times by a super-diffusive motion associated with the directed motion observed during the run phase, in agreement with previous works [39–42]. The ETAMSD was fitted in the interval $0.3 \le \tau \le 2$ s, corresponding to the short-time regime where the run phase is observed, using a power-law dependence, $\langle \Delta r^2(\tau)\rangle = \langle K\rangle \tau^n$ with exponent n ≈ 1.35, where $\langle\,\rangle$ indicates the ensemble average (Fig. 2B). K is a transport coefficient having units μm$^2/s^n$. The same power-law function was used to model all data over the same lag-time interval, corresponding to the regime of short-time dynamics over which all curves present a single, well-defined slope. Note that we did not observe cytotoxycity effects associated with the staining of the bacteria with SYTO9, even at longer times after sample preparation (see Fig. 7 in the SM). We also modeled the ETAMSD using the Ornstein–Uhlenbeck equation [43] (see Fig. 5 in the SM), that allowed us to estimate an average run length of approximately 5.5 μm. For the pure PVA hydrogel (CT 0%), that presents pores of average diameter of a few μm (Fig. 1), some trajectories still evidence directed motion, however others indicate rather random motion (Fig. 2A). The ETAMSD becomes less super-diffusive (Fig. 2B), as indicated by the reduction in the exponent n ≈ 1.25. The fit with the Ornstein–Uhlenbeck equation (Fig. 5 in the SM) in this case yields a run length of about 2 μm, that is comparable with the pore size. These findings are consistent with previous studies on the same bacteria confined in porous PEG hydrogels [39]. Progressively increasing the CT content trajectories do not show any longer directed motion, rather random motion, and indicate increasingly limited excursions (Fig. 2A, additional plots in Fig.3 of the SM). The ETAMSD correspondingly becomes first diffusive and then subdiffusive at intermediate CT content, and finally almost flat for CT 70% (Fig. 2B). This suggests a progressive qualitative transition in the nature of bacterial motions and an overall suppression of the bacterial dynamics. This qualitative trend of $\langle \Delta r^2(\tau)\rangle$ is confirmed by the values of the time-dependent diffusion coefficient, $D(\tau) = n\langle K\rangle \tau^{n-1}$ calculated for $\tau = 1$ s, that we indicate as D^*, and the exponent n, both monotonically decreasing with increasing CT content (Fig. 2C,D) [44,45]. Errors on K and n were obtained from the fits of equation $\langle \Delta r^2(\tau)\rangle = \langle K\rangle \tau^n$, and were propagated to obtain the error on D^*. It is interesting to note that the observed decrease of the average motility of the bacteria is not coherent with changes in the average pore size of the system, that remains similar or even slightly increases with increasing CT content, as demonstrated in the previous section. It therefore suggests that the observed effect is the result of the interaction

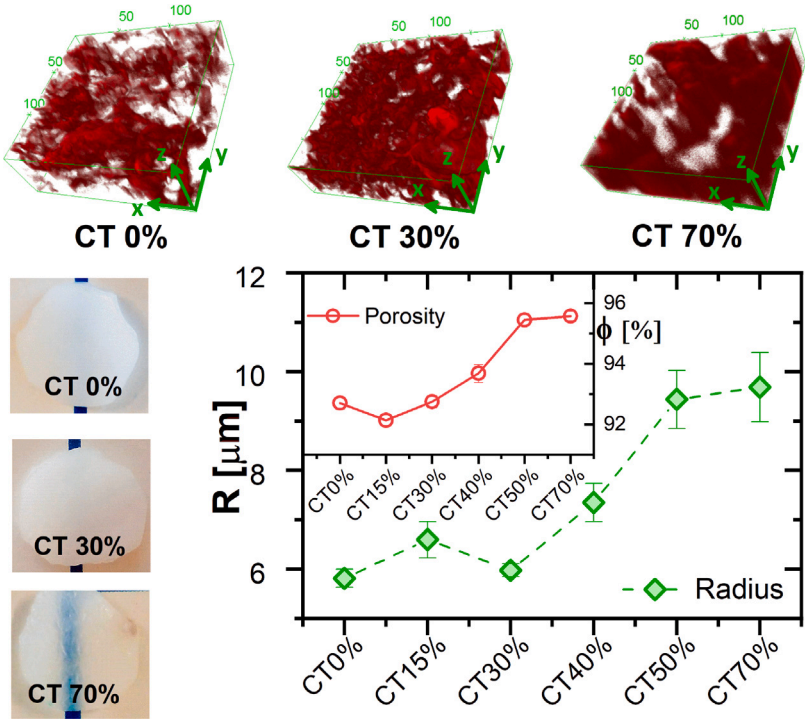

Fig. 1. Top: Exemplary 3D stacks from confocal microscopy of fluorescently-labeled hydrogels with CT contents equal to 0%, 30% and 70% (as indicated). Right: Average pore radius as a function of CT content, error bars correspond to one standard deviation. Inset: Porosity as a function of CT content, error bars are smaller than symbols. Left: Pictures of the gels for the indicated CT contents, reprinted from Ref. [26] used under Creative Commons CC-BY 4.0 license.

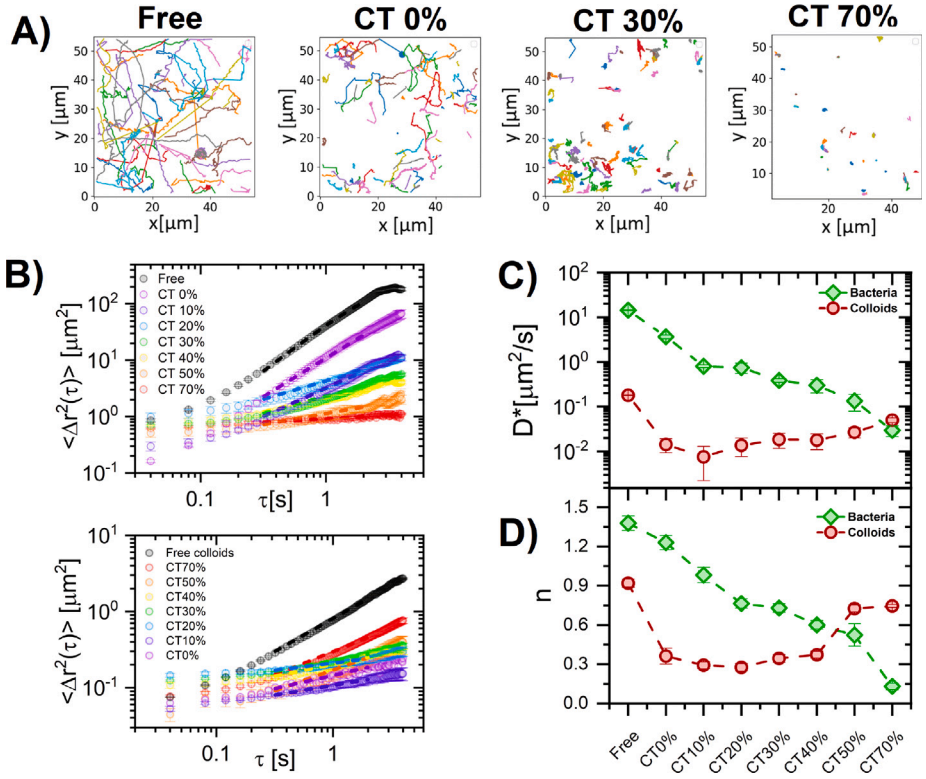

Fig. 2. (A) Trajectories of bacteria measured for $\tau = 1$ s and four different conditions: free (unconfined) and confined within hydrogels with CT content of 0%, 30% and 70% (as indicated). (B) MSD of bacteria (top) and colloidal spheres (bottom) under unconfined and confined conditions. The dotted lines represent fits according to equation: $\langle \Delta r^2(\tau) \rangle = \langle K \rangle \tau^n$. (C) Time-dependent diffusion coefficient calculated for $\tau = 1$ s, D^* and (D) Power-law exponent n extracted from fits of the MSDs in B, as a function of CT content. Error bars in panels B, C and D correspond to one standard deviation.

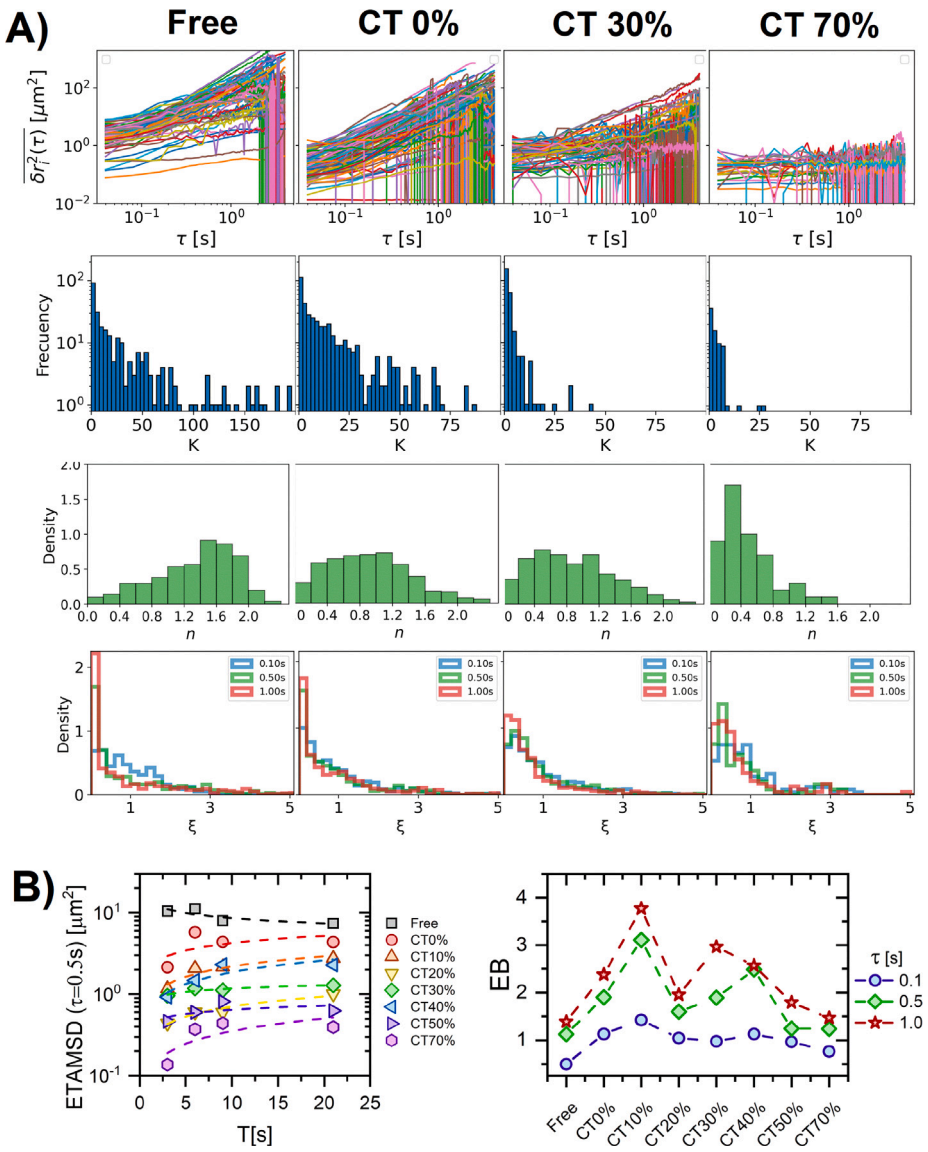

Fig. 3. (A) The top to bottom rows show individual MSDs and the distributions of K, n and ξ for free bacteria and for bacteria in gels with chitosan concentrations of 0%, 30%, and 70%, as indicated. (B) Left: Ensemble-averaged, time-averaged MSD (ETAMSD) calculated at $\tau = 0.5$ s for all samples (as indicated); Lines represent fits to a power-law dependence. Right: Ergodicity breaking (EB) parameter as a function of chitosan concentration, calculated for τ = 0.1, 0.5 and 1.0 s, as indicated.

between the bacteria and Chitosan. In order to test this interpretation, we performed similar experiments using passive, uncharged colloidal particles (PNIPAM microgels) having size comparable to that of *B. subtilis* ($R_{\mu gel} \approx 1$ μm). The ETAMSDs obtained for microgel particles absorbed within gels with different CT content show a trend that is opposite compared to bacteria (Fig. 2B, bottom): They are sub-diffusive with power-law exponents between 0.2 and 0.3 up to 40% CT content (Fig. 2D), a regime where the hydrogel porosity is almost unchanged, while the exponent increases for larger contents attaining a final value of 0.6 for CT70 (Fig. 2D), where also the average pore size attains its maximum value. Consistently, also the time-dependent diffusion coefficients calculated for $\tau = 1$s show almost constant values, about an order of magnitude lower than unconfined microgel suspensions, up to 40% CT content, while they increase for larger CT contents (Fig. 2D). These findings confirm that porosity should lead to an increase in the bacterial motility with increasing CT content in the absence of specific interactions.

3.3.2. *Individual time averaged MSDs and distributions of motility*

To better understand and classify the anomalous diffusion observed in our experiments we analyzed in more detail the distribution of the individual MSDs of each sample [24,25]. Fig. 3A(top) shows the MSDs of individual bacteria obtained for CT contents equal to 0, 30 and 70%, the same samples previously considered for the analysis of the ETAMSD. The progressive reduction of the motility with increasing CT content already discussed for the ensemble averaged MSD is clear also from these plots. In all cases a broad distribution of the MSDs is evident, however some qualitative differences are present depending on CT content: While for the free bacteria most of the MSDs are super-diffusive, consistent with the run phase of the motility and similar to findings for other motile cell systems [25], for the pure PVA hydrogel (CT 0%) one can discern a larger fraction of diffusive or sub-diffusive MSDs. These become dominant for CT 30% and are the only population for CT 70%. Furthermore, the spread of the individual MSDs first increases for CT 0% and 10%, then decreases for larger CT contents. Each individual MSD was analyzed according to the equation $\Delta r^2(\tau) = K\tau^n$. Fig. 3A(middle rows) reports the histograms of K and n values

obtained for the free bacteria and the bacteria absorbed within the 3 selected hydrogels. The distribution of K narrows down to smaller values with increasing CT content, confirming the reduction of the spread qualitatively discussed for the individual MDSs. The distribution of exponents n shifts towards smaller values. It becomes broader for small CT contents, and again narrower for larger values. This indicates the coexistence of dynamics going from superdiffusive to subdiffusive at intermediate CT contents, while the majority of bacteria present subdiffusive motion for large contents of Chitosan. Furthermore, we found a positive correlation between K and n, similar to what observed for passive particles confined in disordered matrices [46] (not shown). We additionally calculated for three different delay times $\tau = 0.1$ s, 0.5 s and 1.0 s the relative deviation of each individual MSD from the ensemble average, that is $\xi(\tau)$ according to Eq. (4), and determined the distribution of values of $\xi(\tau)$ that quantifies the spread of the MDSs. For normal diffusion associated to Brownian motion, the distribution would be a gamma function at $\xi = 1$. As shown in Fig. 3A(bottom) the distributions are asymmetric for all times and CT contents, and not centered around 1, confirming the anomalous diffusion behavior of our samples. Furthermore, the distributions become increasingly skewed towards smaller values with increasing delay time, indicating a stronger deviation from ergodic, diffusive behavior. All distributions present a finite value for $\xi = 0$, a characteristic of anomalous diffusion processes like the weakly non-ergodic continuous-time random walk (CTRW), heterogeneous diffusion [24], transient trapping [47] or motion of bacteria with variable motility [25]. The value also slightly decreases with increasing CT content, while the distribution broadens. The individual MSDs, K, n and $\xi(\tau)$ distributions for other CT contents are reported in Fig.4 of the SM. While the distributions of individual TAMSD show features that are consistent with CTRW or heterogeneous diffusion, the ETAMSD dependence on the lag-time and on the length of the trajectory show deviations from predictions of these models. Indeed, as seen in Fig. 2B, a linear dependence on the lag-time is only approximately observed in one case for the ETAMSD. Furthermore, Fig. 3B (left) reports the values of the ETAMSDs of the samples calculated at $\tau = 0.5$ s as a function of the trajectory length T, showing that the expected scaling T^{n-1} is generally not describing the experimental data. Indeed for the free bacteria the ETAMSD($\tau = 0.5$ s) slightly decreases with increasing T, instead of increasing, while for the sub-diffusive cases for CT > 10% it increases with T instead of decreasing. Values of the exponents α describing the power-law dependence of ETAMSD($\tau = 0.5$ s) on T are reported in Tab.1 of the SM, and compared to $n-1$. These findings suggest that the interplay of different effects, like variation of cell behavior in the strain, separation in populations, combination of confinement and interactions, cannot be easily captured by available anomalous diffusion models.

The variance of the $\xi(\tau)$ distribution, the ergodicity breaking parameter EB calculated according to Eq. (5), is shown in Fig. 3B for the 3 delay times and as a function of CT content. EB is 0 for a purely ergodic process. At the shortest time EB is around 0.5 for free bacteria, indicating a moderate deviation from ergodicity, while it increases to 1 and above for CT 0% and 10%, respectively, then decreases back to 1 and remains approximately constant for all larger CT contents. The EB, however, increases significantly for longer delay times, especially for the bacteria confined within hydrogels. This finding is consistent with results of anomalous diffusion of passive tracers absorbed within hydrogels [46]. Particularly interesting is the finding that the trend is non-monotonic as a function of CT content with a clear maximum observed for CT 10%. This behavior could be the result of a competition between two different effects: confinement and electrostatic interaction. For 0 or small CT content, the main influence on the bacterial motion arises from confinement effects, that lead to an increase of the heterogeneity of the dynamics and a broadening of the MSDs spread, resulting in larger EB values. However, for significant CT amount, the electrostatic interaction between the hydrogel and the bacteria becomes important, while confinement effects are reduced due to the growth of the pore sizes. The dynamics become slower but more homogeneous, leading to a progressive decline of the EB value.

3.3.3. Velocity distributions and reorientation rate

The progressive loss of motility of bacteria absorbed within hydrogels containing increasingly larger amounts of CT is confirmed by additional analyses of the velocity distributions, reorientation rate and confinement ratio. These were calculated in TrackMate [33] starting from the trajectories obtained by particle tracking. The mean velocity was calculated as the average of the instantaneous velocities between consecutive positions along a trajectory. For each pair of successive spots starting at time t_i, a link velocity is first defined as

$$v_i = \frac{d_{i,i+1}}{\Delta t_{i,i+1}} \tag{6}$$

where $d_{i,i+1}$ is the distance between two consecutive positions and $\Delta t_{i,i+1}$ is the corresponding time interval. The mean velocity is then obtained as the average over all N steps:

$$\mathrm{v}_{\mathrm{mean}} = \frac{1}{N}\sum_{i=1}^{N} v_i. \tag{7}$$

The reorientation rate γ_j of individual trajectories was defined according to Eq. (8), where i and $i+1$ are two consecutive steps between which the reorientation angle is $\theta_{i,i+1}$, N is the total number of reorientation events, and Δt_j is the duration of the trajectory.

$$\gamma_j = \frac{\sum_i \theta_{i,i+1}}{N \Delta t_j} \tag{8}$$

The average reorientation rate corresponds to the mean of the γ_j of all trajectories, and errors on the average were estimated as one standard deviation

The confinement ratio $(\mathrm{Cfn.Ratio})_j$ of a trajectory reflects the "efficiency" of the trajectory in moving away linearly from its starting point; it therefore reflects the presence of physical obstacles or chemical factors that can cause the trajectory to become increasingly tortuous. It is defined by Eq. (9), where d_{j0} is the linear distance between the starting and final point and $\sum_i d_{i,i+1}$ indicates the total distance traveled along the trajectory.

$$(\mathrm{Cfn.Ratio})_j = \frac{d_{j0}}{\sum_i d_{i,i+1}} \tag{9}$$

The average Cfn. Ratio was calculated as the mean value of the $(\mathrm{Cfn.Ratio})_j$ of all trajectories, and errors on the average were estimated as one standard deviation.

Fig. 4A shows the mean velocity distributions for increasing CT content: The distribution obtained for free swimming bacteria is centered around $\mathrm{v}_{\mathrm{mean}} \approx 20$ μm/s, consistent with previous findings [39]. For CT contents from 0% to 20% the distribution shifts towards smaller $\mathrm{v}_{\mathrm{mean}}$ values and broadens, consistent with the observations on the distributions of the K and EB coefficients. For larger CT contents the shift to lower values is more moderate and the distributions become again narrower. This confirms that the distribution of motility is maximally heterogeneous at small to intermediate CT contents. In addition, for all confined cases we observe the appearance of a second population of low velocities, that increases and shifts towards increasingly smaller values with increasing CT content, again in agreement with the distributions of individual MSDs. At the same time, the reorientation rate increases, indicating that bacteria try to reorient more often to escape from local constraints, either induced by confinement or electrostatic interactions. Consistent with the literature, rod-shaped bacteria with uniformly distributed flagella as *B. subtilis* can modulate the reorientation speed through clockwise rotation of one or more filament motors; allowing rotation event with a turning angle that can range from 30 to 90 μm/s [48,49]. Correspondingly, the average value of the confinement ratio, that is defined as the ratio between the net displacement along a bacterial trajectory and the total displacement, decreases with increasing CT content, indicating the transition from directed to random motion and progressive arrest.

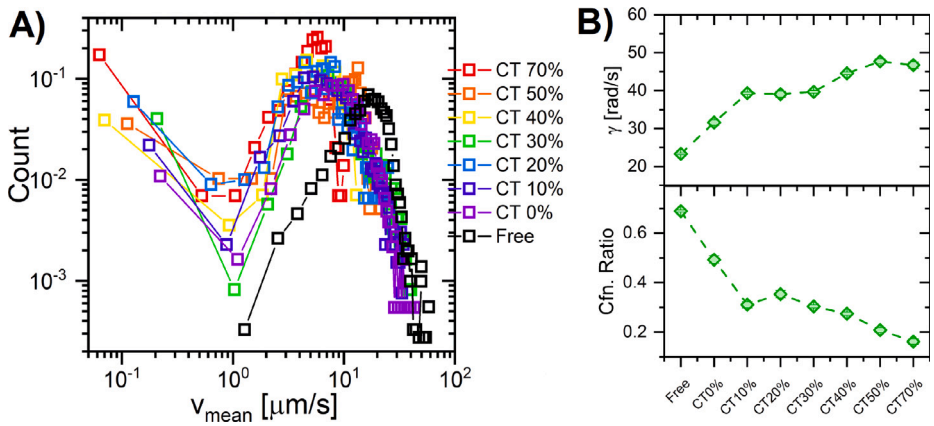

Fig. 4. (A) Mean velocity distribution of bacteria absorbed within hydrogels containing different amounts of chitosan (as indicated). Error bars are smaller than symbols. (B) Average reorientation rate (top) and confinement ratio (bottom) as a function of CT content. Error bars correspond to one standard deviation.

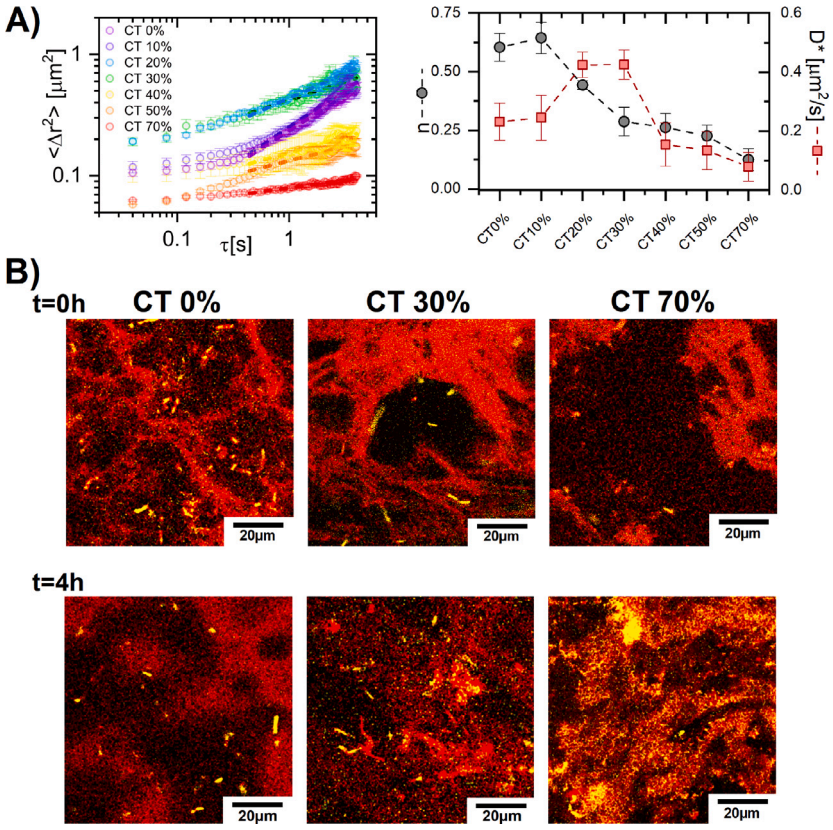

Fig. 5. (A) (Left) ETAMSDs of bacterial dynamics, measured 4 h after the bacteria were placed in the HG. Lines are fits to eq. $\langle \Delta r^2(\tau) \rangle = \langle K \rangle \tau^n$. (Right) Exponent n (left y-axis) and D^* (right y-axis) extracted from the fits in the left panel. Error bars correspond to one standard deviation. (B) Images for the initial state at t = 0 h (top) and after 4 h in HG (bottom), for three different Chitosan contents: 0%, 30%, and 70%, as indicated.

3.3.4. Effects of interaction time on the motility

We compared the bacterial dynamics measured immediately after the absorption of the bacteria within the hydrogels with those obtained 4 h later. The ETAMSDs obtained after 4 h are in all cases significantly reduced compared to the ones measured initially (Fig. 5-A, left), and sub-diffusive, as indicated by the fitted n values (Fig. 5-A, right). The D^* values obtained from modeling the MSDs for $\tau > 0.4$s confirm the strong reduction of motility (Fig. 5-A, right). Errors on the n and D^* values were obtained from fits. The origin of these differences is clear when confronting the images obtained at the two times (Fig. 5-B): Shortly after absorption (top row) the bacteria occupy the pores within the hydrogels, and move within them, with only a small fraction of them that appears to be attached to the hydrogel surface for CT > 40%. No clear evidence of distorted/damaged bacterial bodies is present, as deduced from direct inspection of the images. Instead, after 4 h (bottom row) one can see, except for CT 0%, a significant fraction of bacteria lying on the hydrogel surface, which becomes larger with increasing CT amount. In addition, distorted bacterial bodies are already observed at CT content equal to 20% and become the majority for 70% CT content. Images for additional composition can be found in Fig.6 of the SM. Therefore, the observed reduction in the motility is the effect of the antibacterial action of CT, leading to attachment of the bacteria to the hydrogel surface through electrostatic interaction, where the bacterial membranes are progressively disrupted. However, the amount of damaged bacteria within 4 h is finely tuned by the

hydrogel composition. Additional measurements at intermediate time will be performed in the future to precisely assess the timescale of the electrostatic trapping and live/dead assays to precisely determine the fraction of damaged/dead bacteria.

4. Conclusions

We investigated how the run-and-tumble motility of exemplary gram positive bacteria, *B. subtilis*, is affected by the interaction with antimicrobial hydrogels containing different amounts of chitosan. This was achieved by analyzing the trajectories obtained through particle tracking analysis of confocal microscopy images of bacteria absorbed within the hydrogels. Shortly after absorption, the bacterial motility was found to reduce with increasing chitosan content, changing also its nature from superdiffusive to diffusive and sub-diffusive, with also the mean velocity that reduces while the reorientation rate increases. A detailed analysis of the individual MSD distributions evidenced that when bacteria are absorbed within hydrogels, anomalous diffusion is always observed, and the spread of the MSDs reveals the presence of large dynamical heterogeneities. This spread, as indicated by the ξ distributions and determined by the ergodicity breaking parameter calculated at intermediate and long times, shows a non-monotonic trend with a maximum at 10% chitosan content, also consistent with the variation of the width of the velocity distributions. The trend was interpreted in terms of the CT-content dependent interplay of confinement effects and electrostatic interactions. At small CT contents, i.e. for moderate interaction, the heterogeneity of the dynamics is large, since populations with very different motility are present: bacteria that still exhibit run-and-tumble motility while others slowdown or become almost arrested due to confinement effects and entrapment on the surface of the hydrogel. However, with increasing CT content, i.e. for stronger interactions, the population of entrapped bacteria with small, similar motility rapidly grows, while confinement effect should eventually slightly reduce, resulting in a reduction of the spread of the MSDs. We confirmed that the effect is linked to the CT-induced interactions by performing analogous measurements on neutral microgel particles of comparable size, that show an opposite trend associated with variation of the degree of confinement as a function of CT content. At the early stage of interaction investigated in this work, the number of damaged/dead cells is very small even for the largest CT contents. If the same experiments are performed 4 h after absorption of the bacteria within the hydrogels, the dynamics are sub-diffusive for all CT contents and the amount of damaged/dead cells strongly increases, but is still modulated by the CT content. Our results thus demonstrate that the antimicrobial activity of chitosan-based hydrogels can be estimated by motility measurements and can be quantitatively tuned in terms of temporal action and strength by the chitosan content. We expect these results to open the way to the development of chitosan-based materials with precisely controlled antimicrobial properties. Additional tests for different interaction times will be needed to precisely establish the critical timescale of the antimicrobial action. Furthermore, live/dead assays using propidium iodide and traditional cytotoxicity tests will be performed in the future to quantitatively assess the antimicrobial action of the gels.

CRediT authorship contribution statement

F. Soto-Bustamante: Writing – review & editing, Visualization, Methodology, Investigation, Formal analysis, Data curation, Conceptualization. **G. Bassu:** Writing – review & editing, Visualization, Methodology, Investigation, Formal analysis, Data curation, Conceptualization. **M. Laurati:** Writing – review & editing, Writing – original draft, Validation, Supervision, Resources, Project administration, Methodology, Funding acquisition, Conceptualization.

Declaration of competing interest

The authors declare that they have no known competing financial interests or personal relationships that could have appeared to influence the work reported in this paper.

Acknowledgments

F. S.-B. and M.L. acknowledge support from the European Union-PON Research and Innovation 2014–2020, Article 24, paragraph 3a, Law No. 240 of 30 December 2010, as amended, and Ministerial Decree No. 1062 of 10 August 2021. G.B. and M.L. acknowledge support from the project "QCMICRO", funded by "Regione Toscana" within the program "Giovanisì". G.B. and M.L. gratefully acknowledge the support of the ISIS@MACH ITALIA Research Infrastructure, the hub of ISIS Neutron and Muon Source (UK), [MUR official registry U. 0008642.28-05-2020 – 16th April 2020]. IM@IT is listed in the Italian Ministry of University and Research's Piano Nazionale delle Infrastrutture di Ricerca (PNIR 2021–2027) "in the broader notion of ISIS", and ISIS Facility and IM@IT are jointly listed in high priority RI's (see Table 6 page 30, note 38, PNIR in 2021–2027). All authors acknowledge the Biological Laboratory of the Department of Chemistry at the University of Florence, in particular Dr S. Tilli for laboratory assistance and scientific support, and partial support from Consorzio per lo Sviluppo dei Sistemi a Grande Interfase (CSGI).

Appendix A. Supplementary data

Supplementary material related to this article can be found online at https://doi.org/10.1016/j.ijbiomac.2026.152929.

Data availability

Data will be made available on request.

References

[1] M.-T. Yen, J.-H. Yang, J.-L. Mau, Antioxidant properties of chitosan from crab shells, Carbohydr. Polymers 74 (4) (2008) 840–844, http://dx.doi.org/10.1016/j.carbpol.2008.05.003, https://www.sciencedirect.com/science/article/pii/S0144861708002452.

[2] S. Kim, Competitive biological activities of chitosan and its derivatives: Antimicrobial, antioxidant, anticancer, and anti-inflammatory activities, Int. J. Polym. Sci. 2018 (1) (2018) 1708172, http://dx.doi.org/10.1155/2018/1708172, arXiv:https://onlinelibrary.wiley.com/doi/pdf/10.1155/2018/1708172 https://onlinelibrary.wiley.com/doi/abs/10.1155/2018/1708172.

[3] H. Moldovan D. Gheorghiță, A. Robu, E. Grosu A.-I. Bița, A. Antoniac, I. Corneschi, I. Antoniac, A.D. Bodog, C.I. Băcilă, Chitosan-based biomaterials for hemostatic applications: A review of recent advances, Int. J. Mol. Sci. 24 (13) (2023) http://dx.doi.org/10.3390/ijms241310540, https://www.mdpi.com/1422-0067/24/13/10540.

[4] M. Kong, X.G. Chen, K. Xing, H.J. Park, Antimicrobial properties of chitosan and mode of action: A state of the art review, 144, (1) 2010, pp. 51–63, http://dx.doi.org/10.1016/j.ijfoodmicro.2010.09.012, The 16th CBL (Club des Bactéries Lactiques) Symposium, May 2009, Toulouse, France. https://www.sciencedirect.com/science/article/pii/S0168160510005167,

[5] A. Bernkop-Schnürch, S. Dünnhaupt, Chitosan-based drug delivery systems, Eur. J. Pharmaceut. Biopharmaceut. Off. J. Arbeitsgemeinschaft Fur Pharm. Verfahrenstechnik E. V 81 (3) (2012) 463–469, http://dx.doi.org/10.1016/j.ejpb.2012.04.007.

[6] J. Shah, D. Patel, D. Rananavare, D. Hudson, M. Tran, R. Schloss, N. Langrana, F. Berthiaume, S. Kumar, Recent advancements in chitosan-based biomaterials for wound healing, J. Funct. Biomater. 16 (2) (2025) http://dx.doi.org/10.3390/jfb16020045, https://www.mdpi.com/2079-4983/16/2/45.

[7] I.-Y. Kim, S.-J. Seo, H.-S. Moon, M.-K. Yoo, I.-Y. Park, B.-C. Kim, C.-S. Cho, Chitosan and its derivatives for tissue engineering applications, Biotech. Adv. 26 (1) (2008) 1–21, http://dx.doi.org/10.1016/j.biotechadv.2007.07.009, https://www.sciencedirect.com/science/article/pii/S0734975007000948.

[8] C. Duan, X. Meng, J. Meng, M.I.H. Khan, L. Dai, A. Khan, X. An, J. Zhang, T. Huq, Y. Ni, Chitosan as a preservative for fruits and vegetables: A review on chemistry and antimicrobial properties, J. Bioresour. Bioprod. 4 (1) (2019) 11–21, http://dx.doi.org/10.21967/jbb.v4i1.189, https://www.sciencedirect.com/science/article/pii/S2369969820300335.

[9] A. Guarnieri, M. Triunfo, C. Scieuzo, D. Ianniciello, E. Tafi, T. Hahn, S. Zibek, R. Salvia, A. De Bonis, P. Falabella, Antimicrobial properties of chitosan from different developmental stages of the bioconverter insect hermetia illucens, Sci. Rep. 12 (1) (2022) 8084, http://dx.doi.org/10.1038/s41598-022-12150-3.
[10] C.-L. Ke, F.-S. Deng, C.-Y. Chuang, C.-H. Lin, Antimicrobial actions and applications of chitosan, Polymers 13 (6) (2021) http://dx.doi.org/10.3390/polym13060904, https://www.mdpi.com/2073-4360/13/6/904.
[11] V.S. Mirbagheri, A. Alishahi, G. Ahmadian, S.M. Ojagh S.H. Hashemi Petroudi, G. Romanazzi, Toward understanding the antibacterial mechanism of chitosan: Experimental approach and in silico analysis, Food Hydrocolloids 147 (2024) 109382, http://dx.doi.org/10.1016/j.foodhyd.2023.109382, https://www.sciencedirect.com/science/article/pii/S0268005X23009281.
[12] L.M. Hemmingsen, N. Škalko-Basnet, M.W. Jøraholmen, The Expanded Role of Chitosan in Localized Antimicrobial Therapy., Mar. Drugs 19 (12) (2021) http://dx.doi.org/10.3390/md19120697.
[13] P. Feng, Y. Luo, C. Ke, H. Qiu, W. Wang, Y. Zhu, R. Hou, L. Xu, S. Wu, Chitosan-based functional materials for skin wound repair: Mechanisms and applications, Front. Bioeng. Biotechnol. 9 (2021) 650598.
[14] M.A. Matica, F.L. Aachmann, H. Sletta A. Tøndervik, V. Ostafe, Chitosan as a wound dressing starting material: Antimicrobial properties and mode of action, Int. J. Mol. Sci. 20 (23) (2019) 5889.
[15] C. Dias, A.P. Rauter, Membrane-targeting antibiotics: recent developments outside the peptide space, Futur. Med. Chem. 11 (3) (2019) 211–228.
[16] D. Maršík, O. Mat'átková, A. Kolková, J. Masák, Exploring the antimicrobial potential of chitosan nanoparticles: synthesis, characterization and impact on pseudomonas aeruginosa virulence factors, Nanoscale Adv. 6 (12) (2024) 3093–3105, http://dx.doi.org/10.1039/d4na00064a.
[17] A.T. Bernal-Mercado, J. Juarez, M.A. Valdez, J.F. Ayala-Zavala, D. Encinas-Basurto C.L. Del-Toro-Sánchez, Hydrophobic Chitosan Nanoparticles Loaded with Carvacrol against Pseudomonas aeruginosa Biofilms, Mol. (Basel, Switzerland) 27 (3) (2022) http://dx.doi.org/10.3390/molecules27030699.
[18] F. Hong, P. Qiu, Y. Wang, P. Ren, J. Liu, J. Zhao, D. Gou, Chitosan-based hydrogels: From preparation to applications, a review, Food Chem.: X 21 (2024) 101095, http://dx.doi.org/10.1016/j.fochx.2023.101095, https://www.sciencedirect.com/science/article/pii/S2590157523005382.
[19] J. Yang, M. Shen, Y. Luo, T. Wu, X. Chen, Y. Wang, J. Xie, Advanced applications of chitosan-based hydrogels: From biosensors to intelligent food packaging system, Trends Food Sci. Technol. 110 (2021) 822–832, http://dx.doi.org/10.1016/j.tifs.2021.02.032, https://www.sciencedirect.com/science/article/pii/S0924224421001394.
[20] H. Liu, C. Wang, C. Li, Y. Qin, Z. Wang, F. Yang, Z. Li, J. Wang, A functional chitosan-based hydrogel as a wound dressing and drug delivery system in the treatment of wound healing., RSC Adv. 8 (14) (2018) 7533–7549, http://dx.doi.org/10.1039/c7ra13510f.
[21] A. Dsouza, C. Constantinidou, T.N. Arvanitis, D.M. Haddleton, J. Charmet, R.A. Hand, Multifunctional composite hydrogels for bacterial capture, growth/elimination, and sensing applications, ACS Appl. Mater. Interfaces 14 (42) (2022) 47323–47344, http://dx.doi.org/10.1021/acsami.2c08582.
[22] N. Wadhwa, H.C. Berg, Bacterial motility: machinery and mechanisms, Nat. Rev. Microbiol. 20 (3) (2022) 161–173, http://dx.doi.org/10.1038/s41579-021-00626-4, https://www.nature.com/articles/s41579-021-00626-4.
[23] S. Mukherjee, D.B. Kearns, The structure and regulation of flagella in bacillus subtilis, Annu. Rev. Genet. 48 (Volume 48, 2014) (2014) 319–340, http://dx.doi.org/10.1146/annurev-genet-120213-092406, https://www.annualreviews.org/content/journals/10.1146/annurev-genet-120213-092406.
[24] R. Metzler, J.-H. Jeon, A.G. Cherstvy, E. Barkai, Anomalous diffusion models and their properties: non-stationarity, non-ergodi and ageing at the centenary of single particle tracking, Phys. Chem. Chem. Phys. 16 (2014) 24128–24164, http://dx.doi.org/10.1039/C4CP03465A.
[25] A.G. Cherstvy, O. Nagel, C. Beta, R. Metzler, Non-gaussianity, population heterogeneity and transient superdiffusion in the spreading dynamics of amoeboid cells, Phys. Chem. Chem. Phys. 20 (2018) 23034–23054, http://dx.doi.org/10.1039/C8CP04254C.
[26] F. Soto-Bustamante, G. Bassu, E. Fratini, M. Laurati, Effect of composition and freeze-thaw on the network structure, porosity and mechanical properties of polyvinyl-alcohol/chitosan hydrogels, Gels 9 (5) (2023) http://dx.doi.org/10.3390/gels9050396, https://www.mdpi.com/2310-2861/9/5/396.
[27] G. Bassu, M. Laurati, E. Fratini, Microgel dynamics within the 3d porous structure of transparent peg hydrogels, Colloids Surf. B 221 (2023) 112938, http://dx.doi.org/10.1016/j.colsurfb.2022.112938, https://www.sciencedirect.com/science/article/pii/S0927776522006221.
[28] Leibniz Institute DSMZ, 10, 2024, https://www.dsmz.de/collection/catalogue/details/culture/DSM-10. (accessed: 08 January 2026),
[29] D.-G. Ha, S.L. Kuchma, G.A. O'Toole, Plate-based assay for swimming motility, in: Pseudomonas Aeruginosa, in: Methods in Molecular Biology, Vol. 1149 (2014) 59–65, http://dx.doi.org/10.1007/978-1-4939-0473-0_7.
[30] D.B. Allan, T. Caswell, N.C. Keim, C.M. van der Wel, R.W. Verweij, soft-matter/trackpy: Trackpy. http://dx.doi.org/10.5281/zenodo.4682814.
[31] J.C. Crocker, D.G. Grier, Methods of digital video microscopy for colloidal studies, J. Colloid Interface Sci. 179 (1) (1996) 298–310, http://dx.doi.org/10.1006/jcis.1996.0217, https://linkinghub.elsevier.com/retrieve/pii/S0021979796902179.
[32] T. Wagner, A. Kroll, C.R. Haramagatti, H.G. Lipinski, M. Wiemann, Classification and segmentation of nanoparticle diffusion trajectories in cellular micro environments, PLoS ONE 12 (1) (2017) 1–20, http://dx.doi.org/10.1371/journal.pone.0170165.
[33] J.-Y. Tinevez, N. Perry, J. Schindelin, G.M. Hoopes, G.D. Reynolds, E. Laplantine, S.Y. Bednarek, S.L. Shorte, K.W. Eliceiri, TrackMate: An open and extensible platform for single-particle tracking, Methods 115 (2016) (2017) 80–90, http://dx.doi.org/10.1016/j.ymeth.2016.09.016, https://linkinghub.elsevier.com/retrieve/pii/S1046202316303346.
[34] D. Ershov, M. s. Phan, S.U. Rigaud J.W. Pylvänäinen, L.L. Blanc, J.R.W. Conway, R.F. Laine, N.H. Roy, D. Bonazzi, G. Jacquemet G. Duménil, J. y. Tinevez, Bringing TrackMate into the era of, 2021, pp. 9–12, http://dx.doi.org/10.1101/2021.09.03.458852.
[35] Z. Wang, N. Mahmood, Preparation and characterization of hydrogels fabricated from chitosan and poly(vinyl alcohol) for tissue engineering applications, ACS Appl. Bio Mater. 7 (8) (2024) 5519–5529, http://dx.doi.org/10.1021/acsabm.4c00642, https://pubs.acs.org/doi/10.1021/acsabm.4c00642.
[36] M.D. Figueroa-Pizano, I. Veláz, F.J. Peñas, P. Zavala-Rivera, A.J. Rosas-Durazo, A.D. Maldonado-Arce, M.E. Martinez-Barbosa, Effect of freeze-thawing conditions for preparation of chitosan-poly(vinyl alcohol) hydrogels and drug release studies, Carbohydr. Polymers 195 (2018) 476–485, http://dx.doi.org/10.1016/j.carbpol.2018.05.004, https://www.sciencedirect.com/science/article/abs/pii/S0144861718305265.
[37] K.F. Jarrell, M.J. McBride, The surprisingly diverse ways that prokaryotes move, Nat. Rev. Microbiol. 6 (6) (2008) 466–476.
[38] A. Bren, M. Eisenbach, How signals are heard during bacterial chemotaxis: protein-protein interactions in sensory signal propagation, J. Bacteriol. 182 (24) (2000) 6865–6873.
[39] G. Bassu, M. Laurati, E. Fratini, Transition from active motion to anomalous diffusion for bacillus subtilis confined in hydrogel matrices, Colloids Surf. B 236 (2024) 113797, http://dx.doi.org/10.1016/j.colsurfb.2024.113797, https://www.sciencedirect.com/science/article/pii/S0927776524000559.
[40] G. Ariel, A. Rabani, S. Benisty, J.D. Partridge, R.M. Harshey, A. Be'Er, Swarming bacteria migrate by lévy walk, Nat. Commun. 6 (1) (2015) 8396.
[41] A. Creppy, E. Clément adn C. Douarche, M.V. d'Angelo, H. Auradou, Effect of motility on the transport of bacteria populations through a porous medium, Phys. Rev. Fluids 4 (1) (2019) 013102.
[42] A. Datta, S. Beier, V. Pfeifer, R. Großmann, C. Beta, Bacterial swimming in porous gels exhibits intermittent run motility with active turns and mechanical trapping, Sci. Rep. 15 (1) (2025) 20320, http://dx.doi.org/10.1038/s41598-025-02741-1, https://www.nature.com/articles/s41598-025-02741-1.
[43] G.H. P Nguyen, R. Wittmann, H. Löwen, Active ornstein–uhlenbeck model for self-propelled particles with inertia, J. Phys.: Condens. Matter. 34 (3) (2021) 035101, http://dx.doi.org/10.1088/1361-648X/ac2c3f.
[44] F. Höfling, T. Franosch, Anomalous transport in the crowded world of biological cells, Rep. Progr. Phys. 76 (4) (2013) 046602.
[45] J.-H. Jeon, A.V. Chechkin, R. Metzler, Scaled brownian motion: a paradoxical process with a time dependent diffusivity for the description of anomalous diffusion, Phys. Chem. Chem. Phys. 16 (30) (2014) 15811–15817.
[46] A.G. Cherstvy, S. Tapa, C.E. Wagner, R. Metzler, Non-Gaussian, non-ergodic, and non-fickian diffusion of tracers in mucin hydrogels, Soft Matter 15 (12) (2019) 2526–2551, http://dx.doi.org/10.1039/C8SM02096E.
[47] X. Wang, Y. Chen, Ergodic property of random diffusivity system with trapping events, Phys. Rev. E 105 (1) (2022) 014106, http://dx.doi.org/10.1103/PhysRevE.105.014106.
[48] H.C. Berg, D.A. Brown, Chemotaxis in Escherichia Coli Analysed By Three-Dimensional Tracking, 239, (5374) 1972, pp. 500–504, http://dx.doi.org/10.1038/239500a0,
[49] M. Theves, J. Taktikos, V. Zaburdaev, H. Stark, C. Beta, A bacterial swimmer with two alternating speeds of propagation, Phys. Rev. Lett. 111 (1) (2013) 018102, http://dx.doi.org/10.1103/PhysRevLett.111.018102.